RSC Advances

ROYAL SOCIETY OF CHEMISTRY

www.rsc.org/advances

Possibility of Majorana signature detecting via a single electron spin implanted in a suspended carbon nanotube resonator

Hua-Jun Chen and Ka-Di Zhu*

Key Laboratory of Artificial Structures and Quantum Control (Ministry of Education), Department of Physics and Astronomy, Shanghai Jiao Tong University, Shanghai 200240, China

(Dated: September 11, 2014)

Abstract

Motivated by recent experimental progress towards the detection and manipulation of Majorana fermions in hybrid semiconductor/superconductor heterostructures, we present a novel proposal based on a suspended carbon nanotube resonator with a single electron spin to probe Majorana fermions in all-optical domain. With this scheme, a possible Majorana signature is investigated via the probe-absorption spectrum, and the coupling strength between Majorana fermion and the single electron spin is also determined. We further show that the carbon nanotube resonator behaved as a phonon cavity is robust for detecting of Majorana fermions. In the proposal, the single electron spin can be considered as a sensitive probe. The proposed optical method here may provide a potential supplement for the detection of Majorana fermions.

*Electronic address: zhukadi@sjtu.edu.cn

I. INTRODUCTION

Currently, the zero-energy modes of Majorana fermions (MFs) have focused a great deal of attention owing to their potential applications in topological quantum computation and non-Abelian braiding [1]. Despite its origin in high energy physics, the analogous Majorana zero mode in the low-energy field of solid state physics has been reported [2]. In the past few years, various systems that might host MFs in condensed matter systems have been proposed [3] and many experimental attempts have also been devoted to identify them [4–10]. According to these attempts, the zero-bias conductance peak [11] as a representative property of Majorana modes is often considered as a Majorana signature. These zero-bias conductance peaks have already been observed in several experiments [6–10, 12]. However, these experimental results can not serve as definitive evidences to prove the existence of MFs in condensed matter systems because the zero-bias conductance peaks can appear due to many other mechanisms [13] such as the zero-bias anomaly due to Kondo resonance [14] and the disorder or band bending in the semiconductor nanowire (SNW) [15]. Therefore, to obtain definitive signatures of MFs, alternative setups or proposals for detecting MFs are necessary.

On the other hand, the suspended carbon nanotubes (CNTs) with characteristics of low mass, high and widely tunable resonance frequencies, high quality factors, and remarkable electronic properties [16] make them have potential applications, such as mechanical signal processing [17], mass and force detectors [18]. In recent years, the investigation of spin-orbit interaction in CNTs has gained significant advances. The vibration frequency of CNT can be probed via using the strong coupling between single electron spin and the mechanical vibration based on spin-orbit interaction in the suspended CNTs [19]. Further, this coupling provides the means for manipulation of the electron spin via microwave irradiation, which paves the way for manipulating the spin degree of freedom [20–25].

For the detection of MFs, quantum dots (QDs) [26] and nanomechanical resonator [27] as an intermediates are also employed to probe Majorana signature via tunneling experiments. We notice that all the theoretical proposals and experimental schemes have focused on electrical methods. While other effective methods such as optical scheme for detecting MFs have received less attention. In the present article, based on the recent experiment by Mourik et al. [7], where a SNW with strong spin-orbit coupling placed in proximity with

a superconductor (SC) under a proper external magnetic field (see Fig.1), we will employ a suspended CNT implanted in a single electron spin to detect MFs. By applying a strong pump field (with the pump frequency ω_c) and a weak probe field (with the probe frequency ω_s) to the single electron spin simultaneously [28], the possible Majorana signature could be probed via the probe absorption spectrum of spin. The optical pump-probe technology has been demonstrated experimentally in several systems [30], which provides an effective way to investigate the light-matter interaction. Based on this technique, the linear and nonlinear optical effect can be studied via the absorption spectrum of the probe field.

Compared with electrical detection schemes where the QDs are coupled to MFs via the tunneling [26], in our optical scheme, there is no contact between the CNT and the hybrid SWN/SC junction, and the interaction between MFs in the SWN/SC junction and single electron spin in CNT is mainly due to the exchange interaction. Since the distance between CNT and MFs can be adjusted by several tens of nanometers, therefore the tunneling between the CNT and MFs can be neglected. The signal change in the absorption spectrum as a possible signature for the MFs is another potential evidence in the hybrid SWN/SC junction. This optical scheme will provide another supplement for the detection of MFs, which is very different from the zero-bias peak in the tunneling experiments. Further, the vibration of CNT acted as a phonon cavity will enhance the probe absorption spectrum significantly and make the MFs more sensitive to be detected.

II. MODEL AND THEORY

Figure 1 presents the schematic setup that will be studied in this work. For the CNT system, in the presence of a magnetic field $\mathbf{B}$ the spin constitutes a well-defined two-level system (TLS). As the CNT vibrates, an effective spin-phonon coupling due to the interaction between spin-orbit interaction will happen [31, 32]. In general, the vibrational modes of nanotube resonator can be treated as the phonon modes. The inset of Fig.1 shows the two-level spin state dressing with the flexural modes of CNT via the spin-phonon coupling. Due to Ref. [33], at long phonon wavelengths the deflection coupling is dominated, while at short wavelengths the deformation potential coupling should be dominated [33]. For simplicity here we only consider the deflection coupling mechanism, but note that the approach can readily be extended to include both effects. The Hamiltonian describing this system is as

follows [22, 25, 33]

$$H_{CNT} = \Delta_{so}\tau_3(\mathbf{S}\cdot\mathbf{r}_{tv})/2 + \Delta^{'}\tau_1 - \mu_{orb}\tau_3(\mathbf{B}\cdot\mathbf{r}_{tv}) + \mu_B(\mathbf{S}\cdot\mathbf{B}), \quad (1)$$

where Δ_{so} and $\Delta^{'}$ represent the curvature enhanced spin-orbit coupling and the inter-valley coupling, respectively. τ_i and S are the Pauli matrices in valley and spin space, $\mathbf{r}_{tv}$ is the tangent vector along the CNT axis, and $\mathbf{B} = Be_z$ is the magnetic field along the axis of the suspended CNT. In order to study how electron spin couples to the quantized mechanical motion of the CNT, we consider only a single polarization of flexural motion. A generic deformation of the CNT with deflection $\digamma(z)$ makes the tangent vector $r_{tv}(z)$ coordinate-dependent. Expanding $r_{tv}(z)$ for small deflections, the coupling terms in Eq. (1) can be rewritten as $\mathbf{S}\cdot\mathbf{r}_{tv}\simeq S_z + (du/dz)S_x$ and $\mathbf{B}\cdot\mathbf{r}_{tv}\simeq B_z + (du/dz)B_x$. Using the creation (annihilation) operator a^+ (a) to describe the quantized flexural phonon mode $\digamma(z) = f(z)l_0(a+a^+)/\sqrt{2}$, where $f(z)$ and l_0 are the waveform and zero-point amplitude of the phonon, we then obtain the Hamiltonian of the suspended CNT system as

$$H_{CNT} = \hbar\omega_e S^z + \hbar\omega_n a^+ a + \hbar g(S^+ a + S^- a^+), \quad (2)$$

where $\hbar\omega_e = \mu_B(B - \Delta_{so}/2\mu_B)$, $S^{\pm}$ (S^z) is the pseudospin operator, B denotes the magnetic field strength, and μ_B is spin magnetic moment. ω_n is the vibrational frequency of the nanotube resonator, and g is the spin-phonon coupling strength in CNT [22, 25].

Although several experiments [4–10] have been reported the possible signatures of MFs in the hybrid SWN/SC heterostructure via electrical methods, there are still some debates whether the signatures are the definite MFs. Hence, other schemes or proposals for probing MFs are indispensable. Here we will try to demonstrate the existence of MFs by using optical method, which can be considered as a supplement for detection of MFs. As each MF is its own antiparticle, the MF operator γ with $\gamma^\dagger = \gamma$ and $\gamma^2 = 1$ to describe MFs is introduced. Suppose that the single electron spin couples to γ_1, the Hamiltonian is written by [26]

$$H_1 = i\hbar\omega_M\gamma_1\gamma_2/2 + i\hbar\beta(S^- - S^+)\gamma_1. \quad (3)$$

To detect the MFs, it is helpful to switch the Majorana representation to the regular fermion one via the exact transformation $\gamma_1 = f^\dagger + f$ and $\gamma_2 = i(f^\dagger - f)$, where f and $f^\dagger$ are the fermion annihilation and creation operators obeying the anti-commutative relation $\left\{f,\, f^\dagger\right\} = 1$. Accordingly, in the rotating wave approximation [34], H_1 can be rewritten

as

$$H_{MF} = \hbar\omega_M(f^\dagger f - 1/2) + i\hbar\beta(S^- f^\dagger - S^+ f), \tag{4}$$

where the first term gives the energy of MF at frequency ω_M, and $\hbar\omega_M = \epsilon_M \sim e^{-l/\xi}$ with the wire length (l) and the superconducting coherent length (ξ). This term is so small which can approach zero when the wire length is large enough. The second term describes the coupling between the nearby MFs and the single electron spin in CNT with the coupling strength β, where the coupling strength is related to the distance between the CNT and the hybrid SWN/SC heterostructure. It should be also noted that the term of non-conservation for energy, i.e. $i\hbar g(S^- f - S^+ f^+)$, is generally neglected. We have made the numerical calculations (not shown in the following figures) and shown that the effect of this term is too small to be considered in our theoretical treatment.

In terms of this scheme, we apply the pump-probe scheme to the single electron spin of the CNT simultaneously. The Hamiltonian of the spin coupled to the two fields is given by [28] $H_p = -\mu \sum_{i=c,s} E_i(S^+ e^{-i\omega_i t} + S^- e^{i\omega_i t})$, where μ is the dipole moment of the exciton, and E_i is the slowly varying envelope of the field. The driven spin system with one microwave field has been realized in hybrid spin-resonator system [29]. Therefore, one can obtain the total Hamiltonian of the hybrid system as $H = H_{CNT} + H_{MF} + H_p$. In a rotating frame at the pump field frequency ω_c, the total Hamiltonian of the system can be rewritten as

$$\begin{aligned} H \;=\; & \hbar\Delta_c S^z + \hbar\Delta_n a^+ a + \hbar\Delta_M f^\dagger f + \hbar g(S^+ a + S^- a^+) + i\hbar\beta(S^- f^\dagger - S^+ f) \\ & -\hbar\Omega_c(S^+ + S^-) - \mu E_s(S^+ e^{-i\delta t} + S^- e^{i\delta t}), \end{aligned} \tag{5}$$

where $\Delta_c = \omega_e - \omega_c$ is the detuning of the exciton frequency and the pump frequency, $\Omega_c = \mu E_c/\hbar$ is the Rabi frequency of the pump field, and $\delta = \omega_s - \omega_c$ is the probe-pump detuning. $\Delta_M = \omega_M - \omega_c$ is the detuning of the MF frequency and the pump frequency. Actually, we have neglected the regular fermion like normal electrons in the nanowire that interacts with the spin in CNT. To describe the interaction between the normal electrons and the spin, we use the tight binding Hamiltonian of the whole wire as [35, 36]: $H_{fs} = \hbar\omega_e S^z + \hbar\sum_k \omega_k c_k^+ c_k + \hbar\lambda\sum_k (c_k^+ S^- + S^+ c_k)$, where c_k and $c_k^\dagger$ are the regular fermion annihilation and creation operators with energy ω_k and momentum k obeying the anti-commutative relation $\left\{c_k,\, c_k^\dagger\right\} = 1$, and λ is the coupling strength between the normal electrons and the CNT (here for simplicity we have neglected the k-dependence of λ as in Ref. [37]).

According to the Heisenberg equation of motion and introducing the corresponding damping and noise terms, we derive the quantum Langevin equations as follows

$$\begin{aligned}\dot{S}^z &= -\Gamma_1(S^z+1/2) - ig(S^+a - S^-a^\dagger) - \beta(S^-f^\dagger + S^+f) \\ &\quad +i\Omega_c(S^+ - S^-) + (i\mu E_s/\hbar)(S^+e^{-i\delta t} - S^-e^{i\delta t}),\end{aligned} \tag{6}$$

$$\dot{S}^- = -(i\Delta_c + \Gamma_2)S^- + 2[i(ga - \Omega_c) + \beta f]S^z - 2i\mu E_s S^z e^{-i\delta t}/\hbar + \hat{\tau}_{in}(t), \tag{7}$$

$$\dot{f} = -(i\Delta_M + \kappa_M/2)f + \beta S^- + \hat{\varsigma}(t), \tag{8}$$

$$\dot{a} = -(i\Delta_n + \kappa/2)a - igS^- + \hat{\xi}(t), \tag{9}$$

where Γ_1 (Γ_2) is the electron spontaneous emission rate (dephasing rate), κ is the decay rate of CNT and κ_M is the decay rate of the MF. $\hat{\tau}_{in}(t)$ is the δ-correlated Langevin noise operator, which has zero mean $\langle\hat{\tau}_{in}(t)\rangle = 0$ and obeys the correlation function $\left\langle\hat{\tau}_{in}(t)\hat{\tau}^+_{in}(t')\right\rangle \sim \delta(t-t')$. The resonator mode of CNT is affected by a Brownian stochastic force with zero mean value, and $\hat{\xi}(t)$ has the correlation function

$$\left\langle\hat{\xi}^+(t)\hat{\xi}(t')\right\rangle = \frac{\kappa}{\omega_n}\int\frac{d\omega}{2\pi}\omega e^{-i\omega(t-t')}[1+\coth(\frac{\hbar\omega}{2\kappa_B T})], \tag{10}$$

where k_B and T are the Boltzmann constant and the temperature of the reservoir of the coupled system. MFs have the same correlation relation as resonator mode of CNT.

To go beyond weak coupling, the Heisenberg operator can be rewritten as the sum of its steady-state mean value and a small fluctuation with zero mean value: $S^z = S^z_0 + \delta S^z$, $S^- = S^-_0 + \delta S^-$, $f = f_0 + \delta f$ and $a = a_0 + \delta a$. And then inserting these operators into the Langevin equations (Eqs. (6)-(9)) and neglecting the nonlinear term, we can obtain two equation sets about the steady-state mean value and the small fluctuation. The steady-state equation set consisting of f_0, a_0 and S^-_0 related to the population inversion ($w_0 = 2S^z_0$) of the electron is determined by

$$\begin{aligned}&\Gamma_1(w_0+1)\{(\Delta_c^2+\Gamma_2^2)(\Delta_M^2+\kappa_M^2/4)(\Delta_n^2+\kappa^2/4) + w_0^2[g^4(\Delta_M^2+\kappa_M^2/4) \\ &\quad +\beta^2(\Delta_n^2+\kappa^2/4) + g^2\beta^2(2\Delta_M\Delta_n + \kappa_M\kappa/4)] \\ &\quad +w_0[g^2(\Delta_M^2+\kappa_M^2/4)(2\Delta_c\Delta_M - \Gamma_2\kappa_M) + \beta^2(2\Delta_c\Delta_M + \Gamma_2\kappa_M)]\} \\ &\quad -2\Omega_c^2 w_0[3\kappa g^2(\Delta_M^2+\kappa_M^2/4) + \kappa_M\beta^2(\Delta_n^2+\kappa^2/4)] \\ &\quad +4\Omega_c^2 w_0\Gamma_2(\Delta_M^2+\kappa_M^2/4)(\Delta_n^2+\kappa^2/4) = 0.\end{aligned} \tag{11}$$

For the equation set of small fluctuation, we make the ansatz [28]

$$\langle \delta O \rangle = O_+ e^{-i\delta t} + O_- e^{i\delta t},\ O = S^z,\ S^-,\ f,\ a. \tag{12}$$

Solving the equation set and working to the lowest order in E_s but to all orders in E_c, we can obtain the linear susceptibility as $\chi^{(1)}_{eff}(\omega_s) = \mu S_+(\omega_s)/E_s = (\mu^2/\hbar\Gamma_2)\chi^{(1)}(\omega_s)$, where $\chi^{(1)}(\omega_s)$ is given by

$$\chi^{(1)}(\omega_s) = \frac{[(d_4^* - h_2 d_3^*) d_1 h_3 - i w_0 d_4^*]\,\Gamma_2}{d_2 d_4^* - h_1 h_3 d_1 d_3^*}, \tag{13}$$

where $b_\mp = \beta/[i(\Delta_M \mp \delta) + \kappa_M/2]$, $c_\mp = -ig/[i(\Delta_n \mp \delta) + \kappa/2]$, $h_1 = [-ig(S_0^{-*} c_- - a_0^*) - \beta(f_0^* + S_0^{-*} b_-) - i\Omega_c]/(\Gamma_1 - i\delta)$, $h_2 = [-ig(a_0 - S_0^- c_+^*) - \beta(S_0^- b_+^* + f_0) + i\Omega_c]/(\Gamma_1 - i\delta)$, $h_3 = iS_0^{-*}/(\Gamma_1 - i\delta)$, $d_1 = 2(iga_0 - i\Omega_c + \beta f_0)$, $d_2 = i(\Delta_c - \delta - w_0 g c_-) + (\Gamma_2 - \beta b_- w_0 - d_1 h_1)$, $d_3 = 2(iga_0 - i\Omega_c + \beta f_0)$, $d_4 = i(\Delta_c + \delta - w_0 g c_+) + (\Gamma_2 - \beta b_2 w_0 - d_3 h_4)$ ($\Re^*$ indicates the conjugate of $\Re$). The imaginary and real parts of $\chi^{(1)}(\omega_s)$ indicate absorption and dissipation, respectively. The quantum Langevin equations of the normal electrons coupled to CNT have the same form as MFs, therefore, we omit their derivations and only give the results in the following section.

III. NUMERICAL RESULTS AND DISCUSSION

For illustration of the numerical results, here we use the realistic parameters [20, 22]: $\kappa = 0.05$MHz, $\Gamma_1 = 0.1$MHz, $\Gamma_2 = 0.05$MHz, and $g = 2\pi \times 0.56$MHz. For MF, there are no experimental values for the lifetime of the MFs and the coupling strength between the electron spin and MF as far as we know. However, according to a few reports [6–10, 12], we expect that the decay rate of the MF is in the range of megahertz and $\kappa_M = 0.1$MHz. For the coupling strength between the electron spin of CNT and nearby MF is related to their distance, we expect the coupling strength $\beta = 0.2$MHz via adjusting the distance between the CNT and the hybrid structure. The single electron spin in CNT couples to the nearby MF and produces the coupled states $|e, n_M\rangle$ and $|e, n_M + 1\rangle$ (n_M denotes the number states of the MFs).

The distinct difference between our work and the previous schemes to detect MFs via electrical measurements is the optical detection. Here we employ the single electron spin in CNT to detect MFs. Single electron spin behaved as ultrasensitive probe is beneficial for identifying the Majorana signature. We first radiate a strong pump field and a weak probe

field on the single electron spin in CNT. Once the single electron spin of CNT coupled to the nearby MF, the signature of MFs can be detected via the probe absorption spectrum. Figure 2 shows the absorption spectrum of the probe field (i.e., the imaginary part of the dimensionless susceptibility $\mathrm{Im}\chi^{(1)}$) as a function of the probe-spin detuning Δ_s ($\Delta_s = \omega_s - \omega_e$) with two different coupling strengths $\beta = 0$ and $\beta = 0.2$MHz. The black solid curve is the result when no MFs in the nanowire. As the MFs appear at the ends of the nanowire, the electron spin in CNT will couple to the nearby MF, which induces the upper level of the state $|e\rangle$ to split into $|e, n_M\rangle$ and $|e, n_M + 1\rangle$. The two peaks presented in Fig.2 with a given coupling strength β indicate the spin-MF interaction. As shown in the low two insets of Fig.2, the left peak signifies the transition from $|g\rangle$ to $|e, n_M\rangle$ while the right peak is due to the transition of $|g\rangle$ to $|e, n_M + 1\rangle$. To determine this signature is the true MFs that appear in the nanowire, rather than the normal electrons that couple with the single electron spin in CNT, we give the numerical results of the normal electrons in the nanowire that couple with the single electron spin as shown in the upper right inset of Fig.2. In order to compare with the MF, the parameters are chosen the same as MFs' parameters. We find that there is no signal in the probe absorption spectrum (see the red solid line in the inset of Fig.2) which means that the splitting of the probe absorption spectrum is the true signature of MFs. Therefore, our result here reveals that the splitting in the probe absorption is a real signature of MF.

With increasing the coupling strength β of single electron spin and MF, the distance of the splitting becomes larger and larger, and the stronger coupling strength induces the wider and deeper dip, which obviously reveals the spin-MF coupling. Figure 3 shows the probe absorption spectrum as a function of detuning Δ_s with three spin-MF coupling constants. We find that the distance of the splitting is twice times larger than the spin-MF coupling strength, which provides a straightforward method to measure the spin-MF coupling strength in this coupled system. The inset of Fig.3 indicates a linear relationship between the distance of the peak splitting and the spin-MF coupling strength. Therefore, the coupling strength can be obtained immediately by directly measuring the distance of two peaks in the probe absorption spectrum.

In order to demonstrate the function of the CNT that enhances the sensitivity for detecting MFs, we should consider the vibration of CNT. Figure 4(a) presents the absorption spectrum of the probe field as a function of the probe detuning Δ_s with several spin-phonon

coupling strengths. In Fig.4(a), three coupling strengthes ($g = 0$, 0.2MHz, and 0.56MHz) are considered. $g = 0$ means that there is no spin-phonon coupling in the suspended CNT, there are still two sharp peaks in the absorption spectrum which has been demonstrated in Fig. 3 indicated the the spin-MF coupling. However, once the spin-phonon coupling turns on, more obvious splitting of the curves can be observed in the absorption spectrum. Here, we consider increasing the coupling strength to the realistic value such as $g = 0.56$MHz [20], the two peaks of the absorption spectrum become more significant than that without the spin-phonon coupling in CNT. This result demonstrates that the vibration of CNT will enhance the probe spectrum and make the MFs more sensitive to be detected. This "phonon cavity" enhanced effect is analogous to the optical cavity enhanced effect in quantum optics [39].

In Fig.4(b), we take the spin-phonon coupling into consideration (the red curve), in which the spin-MF coupling $\beta = 0$ and the spin-phonon coupling $g = 0.56$ MHz. Compared with the condition that the spin-MF coupling $\beta = 0.2$ MHz and the spin-phonon coupling $g = 0.56$ MHz, the spin-MF coupling indeed induces the larger splitting. Return to the quantum Langevin equations, we see that Eqs.(8) and (9) are symmetric with respect to the MFs and the single electron spin. As a consequence, the enhanced effect between the spin-MF coupling and the spin-phonon coupling in the probe absorption spectrum is mutual. Here it should also be noted that in our theoretical model the nanotube resonator is not embedded in the bulk superconducting substrate, so the effect of coupling of the nanotube resonator to the bulk superconducting state should not be considered in the present work. The other effects such as surface electric dipole effects and Stark effects can be neglected in the present calculations due to the ultraclean sample and the very weak interactions in the present experiments [4–10].

IV. CONCLUSION

We have proposed an optical method to detect the Majorana fermions in hybrid semiconductor nanowire/superconductor heterostructures via a suspended carbon nanotube with a single electron spin. Based on this scheme, the coupling strength between the spin and nearby Majorana fermions can be determined via the probe absorption spectrum. Due to the CNT's vibrations, the Majorana fermions become more sensitive to be detectable. The

optical scheme may provide another supplement for detecting Majorana fermions. Finally we hope that our proposed scheme can be realized experimentally in the near future.

V. ACKNOWLEDGMENT

This work was supported by the National Natural Science Foundation of China (Nos. 10974133 and 11274230) and the Basic Research Program of the committee of Science and Technology of Shanghai (No.14JC1491700).

[1] F. Wilczek, *Nat. Phys.,* 2009, **5**, 614. J. Alicea, *Rep. Prog. Phys.,* 2012, **75**, 076501. T. D. Stanescu and S. Tewari, *J. Phys. Condens. Matter,* 2013, **25**, 233201.

[2] J. Alicea, *Nat. Nanotech.,* 2013, **8**, 623. S. R. Elliott and M. Franzy, arXiv:1403.4976 (2014).

[3] N. Read and D. Green, *Phys. Rev. B,* 2000, **61**, 10267. L. Fu and C. L. Kane, *Phys. Rev. Lett.,* 2008, **100**, 096407. Y. Tanaka, T. Yokoyama and N. Nagaosa, *Phys. Rev. Lett.,* 2009, **103**, 107002. Y. Oreg, G. Refael and F. von Oppen, *Phys. Rev. Lett.,* 2010, **105**, 177002. J. D. Sau, S. Tewari, R. M. Lutchyn, T. D. Stanescu and S. Das Sarma, *Phys. Rev. B,* 2010, **82**, 214509. S. Nadj-Perge, I. K. Drozdov, B. A. Bernevig and A. Yazdani, *Phys. Rev. B,* 2013, **88**, 020407(R). J. Klinovaja, P. Stano, A. Yazdani and D. Loss, *Phys. Rev. Lett.,* 2013, **111**, 186805.

[4] L. P. Rokhinson, X. Liu and J. K. Furdyna, *Nat. Phys.,* 2012, **8**, 795.

[5] J. R. Williams, A. J. Bestwick, P. Gallagher, S. S. Hong, Y. Cui, A. S. Bleich, J. G. Analytis, I. R. Fisher and D. Goldhaber-Gordon, *Phys. Rev. Lett.,* 2012, **109**, 056803.

[6] A. Das, Y. Ronen, Y. Most, Y. Oreg, M. Heiblum and H. Shtrikman, *Nat. Phys.,* 2012, **8**, 887.

[7] V. Mourik, K. Zuo, S. M. Frolov, S. R. Plissard, E. P. A. M. Bakkers and L. P. Kouwenhoven, *Science,* 2012, **336**, 1003.

[8] M. T. Deng, C. L. Yu, G. Y. Huang, M. Larsson, P. Caroff and H. Q. Xu, *Nano Lett.,* 2012, **12**, 6414.

[9] H. O. H. Churchill, V. Fatemi, K. Grove-Rasmussen, M. T. Deng, P. Caroff, H. Q. Xu and C. M. Marcus, *Phys. Rev. B,* 2013, **87**, 241401(R).

[10] E. J. H. Lee, X. Jiang, M. Houzet, R. Aguado, C. M. Lieber and S. De Francesch, *Nat. Nanotech.* 2014, **9**, 79.

[11] C. J. Bolech and E. Demler, *Phys. Rev. Lett.,* 2007, **98**, 237002. K. T. Law, P. A. Lee and T. K. Ng, *Phys. Rev. Lett.,* 2009, **103**, 237001. K. Flensberg, *Phys. Rev. B,* 2010, **82**, 180516(R). E. Prada, P. San-Jose and R. Aguado, *Phys. Rev. B,* 2012, **86**, 180503(R). A. Yamakage, K. Yada, M. Sato and Y. Tanaka, *Phys. Rev. B,* 2012, 85, 180509(R).

[12] J. P. Xu, M.-X. Wang, Z. L. Liu, J.-F. Ge, X. Yang, C. Liu, Z. A. Xu, D. Guan, C. L. Gao, D. Qian, Y. Liu, Q.-H. Wang, F.-C. Zhang, Q.-K. Xue and J.-F. Jia, arXiv:1312.7110 (2013).

[13] J. Liu, A. C. Potter, K. T. Law and P. A. Lee, *Phys. Rev. Lett.,* 2012, **109**, 267002. G. Kells, D. Meidan and P. W. Brouwer, *Phys. Rev. B,* 2012, **86**, 100503(R). W. Chang, V. E. Manucharyan, T. S. Jespersen, J. Nygard and C. M. Marcus, *Phys. Rev. Lett.,* 2013, **110**, 217005. D. Rainis, L. Trifunovic, J. Klinovaja and D. Loss, *Phys. Rev. B,* 2013, **87**, 024515.

[14] A. D. K. Finck, D. J. Van Harlingen, P. K. Mohseni, K. Jung and X. Li, *Phys. Rev. Lett.,* 2013, **110**, 126406. E. J. H. Lee, X. Jiang, R. Aguado, G. Katsaros, C. M. Lieber and S. De Franceschi, *Phys. Rev. Lett.,* 2012, **109,** 186802.

[15] D. Bagrets, A. Altland and D. Class, *Phys. Rev. Lett.,* 2012, **109,** 227005.

[16] V. Sazonova, Y. Yaish, H. Üetünel, D. Roundy, T. A. Arias and P. L. McEuen, *Nature,* 2004, **431**, 284. A. K. Hüttel, G. A. Steele, B. Witkamp, M. Poot, L. P. Kouwenhoven and H. S. J. van der Zant, *Nano Lett.,* 2009, **9**, 2547. J. Chaste, M. Sledzinska, M. Zdrojek, J. Moser and A. Bachtold, *Appl. Phys. Lett.,* 2011, **99**, 213502. E. A. Laird, F. Pei, W. Tang, G. A. Steele and L. P. Kouwenhoven, *Nano. Lett.,* 2012, **12**, 193. T. S. Jespersen, K. Grove-Rasmussen, J. Paaske, K. Muraki, T. Fujisawa, J. Nygård and K. Flensberg, *Nat. Phys.,* 2011, **7,** 348. A. Eichler, J. Moser, J. Chaste, M. Zdrojek, I. Wilson-Rae and A. Bachtold, *Nat. Nanotechnol.,* 2011, **6,** 339.

[17] B. Lassagne, Y. Tarakanov, J. Kinaret, D. Garcia-Sanchez and A. Bachtold, *Science,* 2009, **325,** 1107.

[18] B. Lassagne, D. Garcia-Sanchez, A. Aguasca, and A. Bachtold, *Nano. Lett.,* 2008, **8**, 3735. H.-Y. Chiu, P. Hung, H. W. C. Postma and M. Bockrath, *Nano. Lett.,* 2008, **8**, 4342. J. Moser, J. Güttinger, A. Eichler, M. J. Esplandiu, D. E. Liu, M. I. Dykman and A. Bachtold, *Nat. Nano.,* 2013, **8**, 493.

[19] D. Garcia-Sanchez, A. San Paulo, M. J. Esplandiu, F. Perez-Murano, L. Forró, A. Aguasca

and A. Bachtold, *Phys. Rev. Lett.,* 2007, **99**, 085501. S. D. Bennett, S. Kolkowitz, Q. P. Unterreithmeier, P. Rabl, A. C. B. Jayich, J. G. E. Harris and M. D. Lukin, *New J. Phys.,* 2012, **14**, 125004.

[20] F. Kuemmeth, S, llani, D. C. Ralph and P. L. McEuen, *Nature,* 2008, **452,** 448.

[21] O. Arcizet, V. Jacques, A. Siria, P. Poncharal, P. Vincent and S. Seidelin, *Nat. Phys.,* 2011, **7,** 879.

[22] A. Pályi, P. R. Struck, M. Rudner, K. Flensberg, and G. Burkard, *Phys. Rev. Lett.,* 2012, **108,** 206811.

[23] G. A. Steele, F. Pei, E. A. Laird, J. M. Jol, H. B. Meerwaldt and L. P. Kouwenhoven, *Nat. Commun.,* 2012, **4**, 1573.

[24] J. J. Li and K. D. Zhu, *Sci. Rep.,* 2012, **2,** 903.

[25] H. Wang and G. Burkard, arXiv:1405.1347 (2014).

[26] K. T. Law, P. A. Lee and T. K. Ng, *Phys. Rev. Lett.,* 2009, **103**, 237001. D. E. Liu and H. U. Baranger, *Phys. Rev. B,* 2011, **84**, 201308. K. Flensberg, *Phys. Rev. Lett.,* 2011, **106,** 090503. M. Leijnse and K. Flensberg, *Phys. Rev. B,* 2011, **84**, 140501(R). Y. S. Cao, P. Y. Wang, G. Xiong, M. Gong and X. Q. Li, *Phys. Rev. B,* 2012, **86**, 115311. P. Wang, Y. Cao, M. Gong, G. Xiong, X. Q. Li, *Europhys. Lett.* 2013, **103**, 57016. Y. Li, A. Kundu, F. Zhong and B. Seradjeh, arXiv:1402.7353 (2014). S. J. S. da Silva, A. C. Seridonio, J. Del Nero and F. M. Souza, arXiv:1403.3575 (2014). A. C. Seridonio, E. C. Siqueira, F. A. Dessotti, R. S. Machado and M. Yoshida, *J. Appl. Phys.,* 2014, **115**, 063706.

[27] S. Walter, T. L. Schmidt, K. Børkje and B. Trauzettel, *Phys. Rev. B,* 2011, **84,** 224510. S. Walter and J. C. Budich, *Phys. Rev. B,* 2014, **89**, 155431.

[28] R. W. Boyd, Nonlinear Optics (San Diego, CA: Academic, 1992).

[29] S. Kolkowitz, J. A. C Bleszynski, Q. P. Unterreithmeier, S. D. Bennett, P. Rabl, J. G. E.Harris and M. D. Lukin, *Science*, 2012, **335**, 1603.

[30] X. D. Xu, B. Sun, P. R. Berman, D. G. Steel, A. S. Bracker, D. Gammon and L. J. Sham, *Science,* 2007, **317**, 929. S. Weis, R. Rivière, S. Deleglise, E. Gavartin, O. Arcizet, A, Schliesser and T. J. Kippenberg, *Science,* 2010, **330,** 1520. J. D. Teufel, D. Li, M. S. Allman, K. Cicak, A. J. Sirois, J. D. Whittaker and R. W. Simmonds, *Nature,* 2011, **471,** 204.

[31] C. Ohm and C. Stampfer, J. Splettstoesser and M. R. Wegewijs, *Appl. Phys. Lett.,* 2012, **100,** 143103.

[32] K. Flensberg and C. M. Marcus, *Phys. Rev. B,* 2012, **81,** 195418.

[33] M. S. Rudner and E. I. Rashba, *Phys. Rev. B, 2012,* **81,** 125426.

[34] A. Ridolfo, O. D. Stefano, N. Fina, R. Saija and S. Savasta, *Phys. Rev. Lett.,* 2010, **105,** 263601.

[35] G. D. Mahan, Many-Partcle Physics (Plenum Press, New York, 1992).

[36] S. Nadj-Perge, I. K. Drozdov, B. A. Bernevig and A. Yazdani, *Phys. Rev. B,* 2013, **88,** 020407(R).

[37] A. C. Hewson, The Kondo Problem to Heavy Fermions (Cambridge University Press, New York, 1993).

[38] G. A. Steele, A. K. Hüttel, B. Witkamp, M. Poot, H. B. Meerwaldt, L. P. Kouwenhoven and H. S. J. van der Zant, *Science,* 2009, **325,** 1103.

[39] S. Stapfner, L. Ost, D. Hunger, E. M. Weig, J. Reichel and I. Favero, *Appl. Phys. Lett.,* 2013, **102**, 151910.

Figure Captions

Fig.1 Schematic diagram of the proposed setup for optically detecting Majorana fermions. An InSb semiconductor nanowire (SNW) with strong spin-orbit interaction (SOI) in an external aligned parallel magnetic field **B** is placed on the surface of a bulk s-wave superconductor (SC). The two yellow stars at the ends of nanowire represent a pair of Majorana fermions. The nearby Majorana fermion is coupled to a single electron spin of suspended carbon nanotube (CNT) under a strong pump laser and a weak probe laser simultaneously. The inset is an energy-level diagram of the spin coupled to Majorana fermion and the CNT resonator.

Fig.2 The probe absorption spectrum as a function of detuning Δ_s without (black curve) and with (blue curve) spin-MF coupling strengths ($\beta = 0$ MHz and $\beta = 0.2$ MHz). The upper right inset is the normal electrons in the nanowire that couple with the spin at the coupling strength $\lambda = 0.2$ MHz. The low two insets represents the energy level transitions of the left peak and right peak presented in the absorption spectrum. The parameters used are $\Gamma_1 = 0.1$ MHz, $\Gamma_2 = 0.05$ MHz, $\kappa_M = 0.1$ MHz, $\kappa = 0.05$ MHz, $g = 0$ MHz, $\Delta_M = -0.1$ MHz, $\Omega_c^2 = 5 \times 10^{-4}(\text{MHz})^2$ and $\Delta_c = \Delta_n = 0$.

Fig.3 The probe absorption spectrum as a function of detuning Δ_s with several spin-MF coupling strengths ($\beta = 0.1$ MHz, 0.2 MHz, 0.3 MHz). The inset shows linear relationship between the distance of peak splitting and the coupling strength of spin-MF. The other parameters used are the same as in Fig.2.

Fig.4 The probe absorption spectrum as a function of detuning Δ_s. (a) The spin-phonon coupling strengths $g = 0$ MHz, 0.2 MHz, and 0.56 MHz at the spin-MF coupling $\beta = 0.2$MHz. (b) The spin-MF coupling $\beta = 0$ MHz and 0.2 MHz at spin-phonon coupling strength $g = 0.56$ MHz. The other parameters used are the same as in Fig.2.

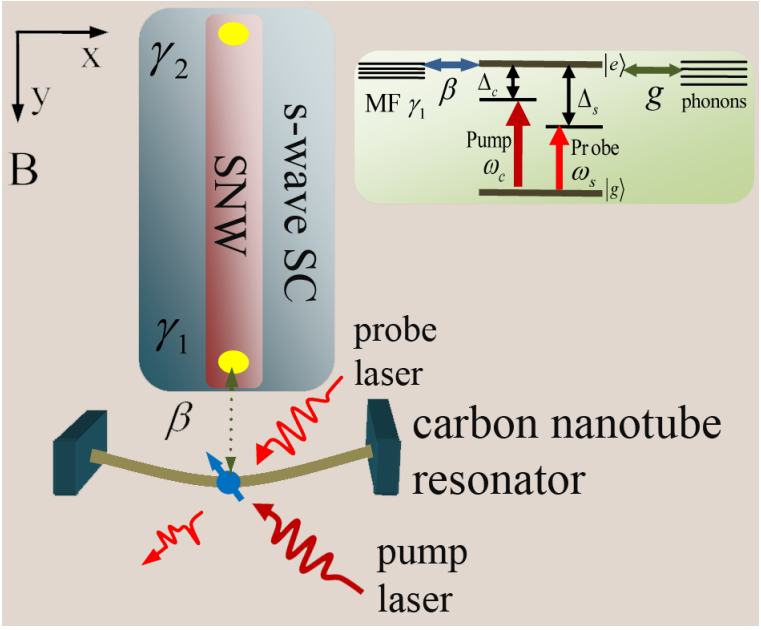

FIG. 1: Schematic diagram of the proposed setup for optically detecting Majorana fermions. An InSb semiconductor nanowire (SNW) with strong spin-orbit interaction (SOI) in an external aligned parallel magnetic field **B** is placed on the surface of a bulk s-wave superconductor (SC). The two yellow spots at the ends of nanowire represent a pair of Majorana fermions. The nearby Majorana fermion is coupled to a single electron spin of the suspended carbon nanotube (CNT) under a strong pump field and a weak probe field simultaneously. The inset is an energy-level diagram of the spin coupled to Majorana fermion and the CNT resonator.

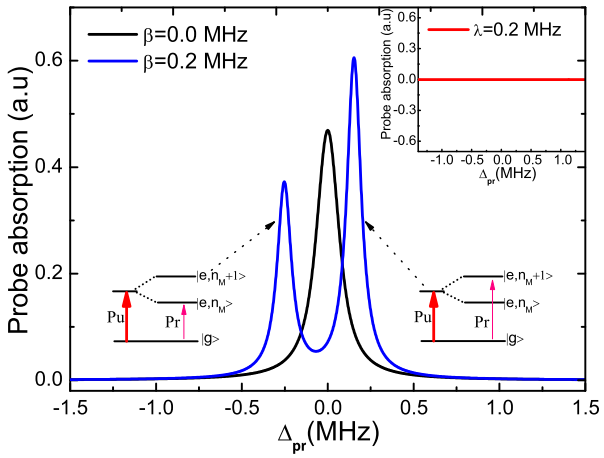

FIG. 2: The probe absorption spectrum as a function of detuning Δ_s without (black curve) and with (blue curve) spin-MF coupling strengths ($\beta = 0$MHz and $\beta = 0.2$MHz). The upper right inset is the normal electrons in the nanowire that couple with the spin at the coupling strength $\lambda = 0.2$ MHz. The low two insets represents the energy level transitions of the left peak and right peak presented in the absorption spectrum. The parameters used are $\Gamma_1 = 0.1$MHz, $\Gamma_2 = 0.05$MHz, $\kappa_M = 0.1$MHz, $\kappa = 0.05$MHz, $g = 0$MHz, $\Delta_M = -0.1$MHz, $\Omega_c^2 = 5 \times 10^{-4}$(MHz)^2 and $\Delta_c = \Delta_n = 0$.

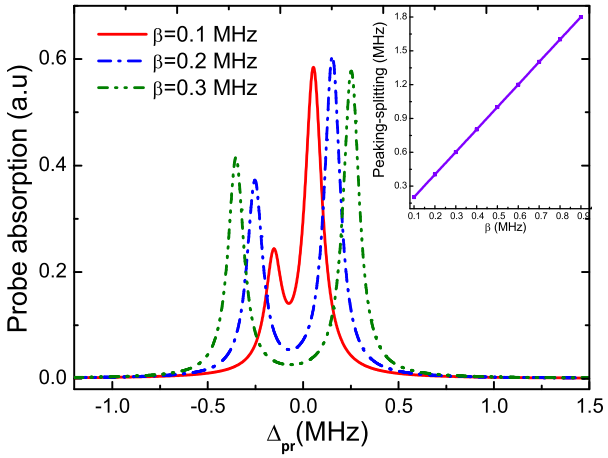

FIG. 3: The probe absorption spectrum as a function of detuning Δ_s with several spin-MF coupling strengths ($\beta = 0.1$MHz, 0.2MHz, 0.3MHz). The inset shows linear relationship between the distance of peak splitting and the coupling strength of spin-MF. The other parameters used are the same as in Fig.2.

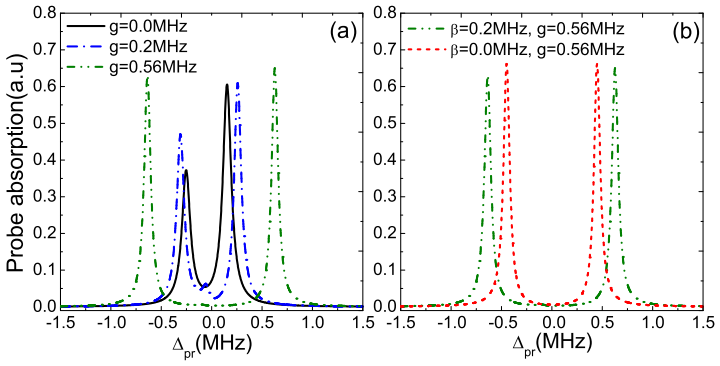

FIG. 4: The probe absorption spectrum as a function of detuning Δ_s. (a) The spin-phonon coupling strengths $g = 0$ MHz, 0.2 MHz, and 0.56 MHz at the spin-MF coupling $\beta = 0.2$ MHz. (b) The spin-MF coupling $\beta = 0$ MHz and 0.2 MHz at spin-phonon coupling strength $g = 0.56$MHz. The other parameters used are the same as in Fig.2.